Flight Verification of Satellite Thermodynamic Analytical Techniques and Application to Manned Spacecraft

LOUIS TESTAGUZZA,* GORDON L. WOLFE,† AND JAMES DIGIORGIO*
Lockheed Missiles and Space Company, Sunnyvale, Calif.

The acquisition of tape-recorded thermal data from an orbiting spacecraft has provided a means of verifying analytical methods and techniques. Continuous monitoring of the temperature excursions of the vehicle structure and components led to an excellent correlation between flight data and analytical predictions. This experiment also provided data, which permitted the study of the thermal behavior and attitude of a nonoriented (tumbling) space vehicle. It was found that inherent attitude perturbations (tumbling) caused by the earth oblateness could be simplified, for thermal purposes, by a pitch-roll analog. A method for determining attitude from temperature data is described. Another significant result demonstrated the importance of knowing the exact location of each temperature sensor; one sensor, located 7.1° from the analytical node center, recorded data 10° to 40°F above predicted temperatures. The instrumentation and ground-space telemetry system used in this experiment are described.

Nomenclature

α = absorptivity, dimensionless
β = solar incidence angle β defined as angle between earth-sun line and orbit plane
ω = solar incidence angle ω defined as angle between earth-sun line and vehicle X axis
β_T = total β
β_i = initial β
Re = earth radius, naut miles
h = altitude, naut miles
i = inclination angle
N_0 = orbit number
ϵ = emissivity, dimensionless
θ = orbital position
ψ = body angle
T = temperature, °R or °F
e = electrical resistance, ohms

Introduction

IN recent years, the utilization of electronic computers and the application of programing techniques have provided the thermodynamicist with an effective tool for analyzing and predicting component and structural temperatures of satellites in orbit. However, the uncertainty of input data (i.e., vehicle equipment internal-power dissipation, conductive and radiation resistances, view factors) has resulted in conservative analytical predictions necessitating imposition of wide temperature tolerances. For critical components with restricted limits, such as man, batteries, and certain mechanical and electronic systems, this wide tolerance has made it necessary to rely on active thermal control methods instead of passive means. Consequently, a greater penalty has resulted in power requirements, weight, reliability, and cost.

Prior to the present experiment, only sporadically acquired, real-time telemetered thermal data have been made available for correlation and verification of analytical predictions. The maximum data-acquisition time during any one pass for a low-altitude orbiting satellite has been approximately 8 min, or 9% of the complete orbit. For certain orbits, such as a north-south pass traversing the Alaska and Hawaii tracking stations' acquisition perimeters, as much as 15 min of data have been acquired. However, the thermal data obtained during any of these short acquisitions have provided only sufficient data to derive the slope of the temperature curve. The maximum or minimum temperature levels experienced were never observed, and the accuracy of predictions were never verified completely for an earth-oriented vehicle.

During a recent satellite flight, a tape recorder that permitted the recording of temperature data throughout complete orbits was flown successfully. The temperature excursions experienced by both structure and components were monitored successfully during both earth-oriented and nonoriented (tumbling) vehicle flight modes.

Experiment Objectives and Description

The primary objective of the flight experiment was to obtain sufficient temperature data from an orbiting vehicle's surface to confirm or improve analytical methods used in prediction and control of spacecraft thermal reactions by accomplishing the following: 1) distribute the instrumentation over the vehicle surface to evaluate the effects of vehicle-environment relationship, 2) obtain data for complete orbits, 3) obtain data over a sufficiently long period of time to evaluate the effects of the earth-sun position change, and 4) provide instrumentation on surfaces having different paint patterns or surface characteristics.

The forward cone-cylinder section of an Agena vehicle surface was instrumented as shown in Fig. 1. Two longitudinal locations, each having 12 radially distributed temperature sensors, gave reasonably good coverage for the vehicle surface in all of the operating modes. Differently painted surfaces were available within the instrumented section because of normal vehicle temperature-control requirements. Instrumentation consisted primarily of semiconductor temperature transducers supplying commutated voltage signals to a magnetic tape recorder. Each sensor was sampled $2\frac{1}{2}$ times/sec. The tape recorder accumulated data for 1.8 consecutive orbits each day. A high-speed readout was initiated by ground station command. The real-time readout was less than 385 sec, allowing some flexibility in acquisition commands. During the data-acquisition periods the ground stations simultaneously received the data being stored via a real-time link.

Presented at the AIAA/USAF-FTC/NASA-FRC Testing of Manned Flight Systems Conference, Edwards Air Force Base, Calif., December 4–6, 1963 (no preprint number; published in bound volume of preprints of the meeting); revision received March 19, 1965.

* Research Specialist. Member AIAA.
† Senior Thermodynamics Engineer.

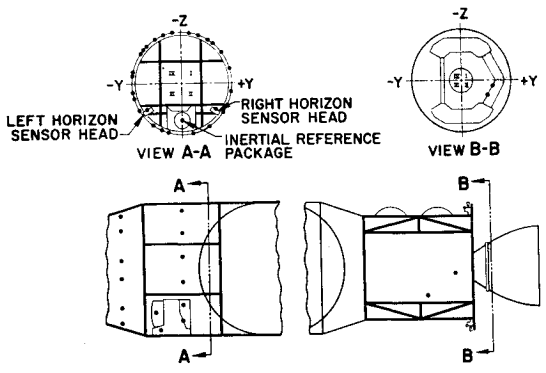

Fig. 1 Tape-recorded temperature sensor locations.

This experiment was carried aboard an Agena vehicle launched from Vandenberg Air Force Base (VAFB) in the spring of 1963 at 1301 Pacific Standard Time (PST) at an inclination angle of 75°. The resulting initial β (the angle between the earth-sun line and the orbit plane of the vehicle) was −50°. The beta angle shift per day was derived from the following equation:

$$\beta_T = \{10[Re/(Re + h)]^{3.5} \cos i + 1\}$$

For each orbit,

$$\beta_T = -50 + 0.194\ (N_0)$$

where N_0 is the orbit number. During the first 3 days the attitude of the vehicle was maintained with the longitudinal axis in the orbit plane and parallel to the surface of the earth. The vehicle then entered a tumbling mode and remained in this mode for 11 days. The total time span covered by this experiment was in excess of 15 days.

Method of Analysis

The temperatures are predicted analytically by conventional electrical analogy networks for radiation and conduction. The network is solved by the Lockheed thermal analyzer program[1,2] on a 7090 IBM digital computer. The procedures are quite well known and widely used by the industry. The external heat rates on the vehicle skins were obtained by means of additional digital programs, including a newly developed routine for predicting instantaneous local rates over the surface of a tumbling vehicle. Heat rates are compared in Fig. 2 for $\beta = -30°$ at two-body angles for the active controlled-attitude mode and the tumbling mode. The pitching and rolling heat rates increase on a body angle that normally would receive only earthshine, some albedo, and little or no direct solar energy. Figure 3 shows maximum and minimum temperature profiles on the vehicle skin for $\beta = -52°$ for both orbital modes. As expected, both maximum and minimum are lower during the pitching/rolling mode. This is most evident on that portion of vehicle skin receiving direct solar energy. The large temperature step at a body angle (ψ) of 45° is caused by the change in surface finish from a low emissivity to a high emissivity. The vehicle equipment arrangement is described by Fig. 4.

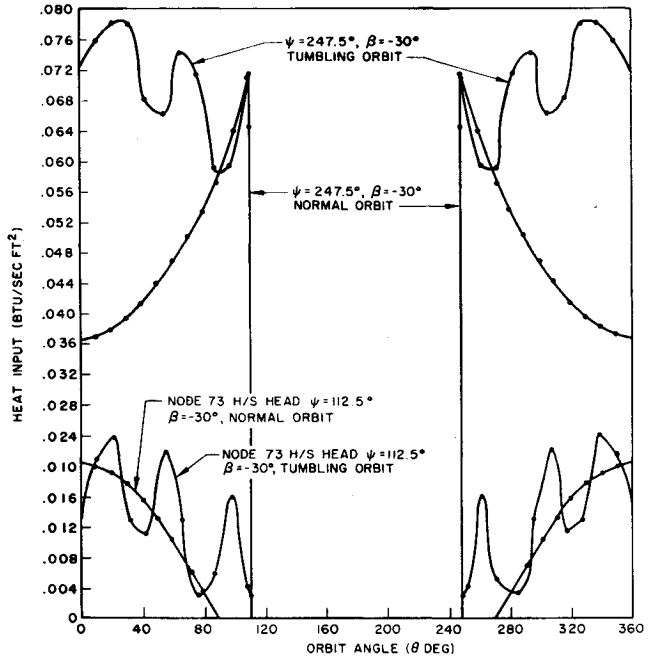

Fig. 2 Comparison of solar and albedo heat rates tumbling vs stable orbit.

Discussion of Data

The need for tape-recorded data is apparent when the limited coverage for low-altitude satellites afforded by present tracking stations is studied. Figure 5 shows the temperature fluctuation of a typical 0.1-in. magnesium skin structure with the real-time data-acquisition times normally available. The figure is for $\beta = -46°$ and shows that two tracking stations, New Hampshire and Vandenberg, can record the lowest temperatures achieved. Because of the earth's inclination, however, this can be done only in the spring. Two other stations, Kodiak and Hawaii, receive data in the middle of the temperature swing because of their latitudes. Note that the coverage afforded would acquire neither the maximum temperatures experienced nor data during the cool-down period. Consequently, confirmation of the analytical treatments has been inadequate, although average temperatures of large thermal capacity equipment have been in general agreement with predictions.

In the present work, tape-recorded data are compared with predictions for two orbits; orbit 25, stabilized and horizontally oriented, and orbit 191, tumbling in the orbit plane, are selected for discussion as typical. The time-dependent structural temperature predictions reflected the influence of mass-material connection of the structure and equipment, external environment, and internal-power dissipation and duty cycles. During orbit 25, the surface element facing the sun experienced the maximum temperature variation as expected (Fig. 6a). The paint pattern selected allowed the temperature at this point to fluctuate from 33° to 153°F. Proceeding counterclockwise around the vehicle surface, the solar heat flux is reduced, and the albedo and earth emission is encountered. Accordingly, the maximum temperature increases, and the minimum temperature rises also, primarily because of earth emission during the "nighttime"

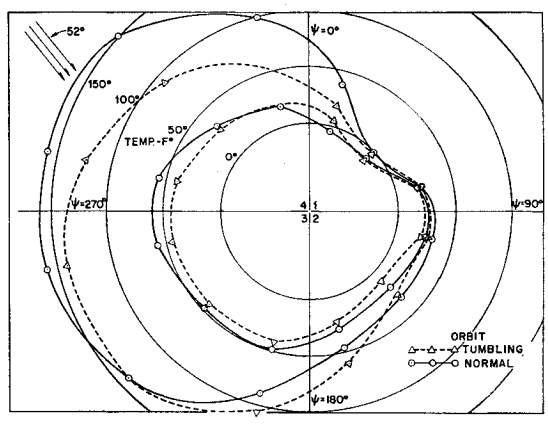

Fig. 3 Maximum and minimum temperature vs vehicle body angle (forward auxiliary rack, $\beta = -52°$).

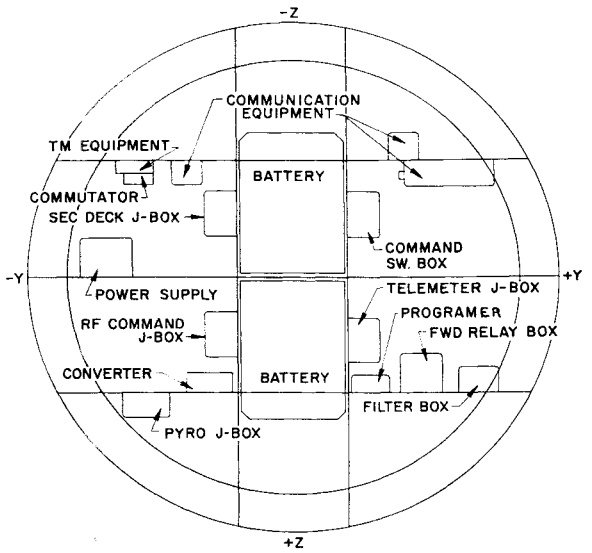

Fig. 4 Equipment bay, forward auxiliary rack (view looking forward).

portion of the orbit. Note the consistent progression of this trend exhibited in both the flight data and the analytical predictions (Figs. 6a–6c). Although the data in Figs. 6b and 6c are from locations close together and in a smoothly changing thermal environment, they are very consistent.

The data comparison continues to be favorable on the earth side of the vehicle where energy from albedo and earth emission alternately predominate as shown in Fig. 6d; also shown are effects of a short exposure of this surface element to the sun as the vehicle comes out of the earth's shadow.

Figure 6e appears to show a greater discrepancy in the data. A review of the instrumentation records showed the sensor to be installed 7° closer to the earth-sun line and to be receiving some solar energy. The mathematical model node center was slightly past the tangency point in the shadow. Therefore, the predicted temperatures show very little change. This data comparison emphasizes the importance of accurate knowledge of sensor location.

Prediction of the temperature histories of the vehicle during its tumbling mode presents new problems. First, an apparent roll oscillation exists in combination with the pitch tumble, affecting local external heat rates. Second, the exact orientation of the pitch axis with respect to the orbit path is not known precisely.

In the absence of other considerations, gyroscopic forces on a tumbling vehicle would tend to force the pitch axis to remain space-oriented; i.e., as the earth moves about the sun, the vehicle pitch axis remains fixed in space and, therefore, shifts with respect to the earth and the orbit plane. Other phenomena, however, such as the gravity gradient, complicate the dynamics of the tumbling vehicle. The gravity gradient itself may force the pitch axis to remain earth-

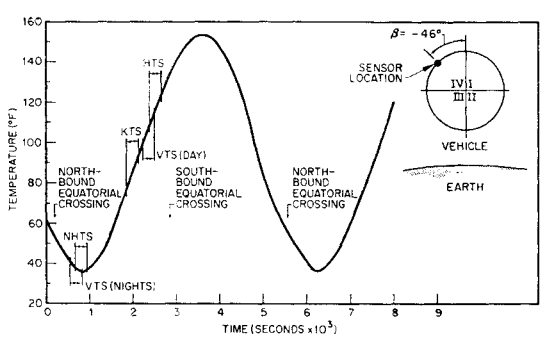

Fig. 5 Typical orbit skin-temperature fluctuation.

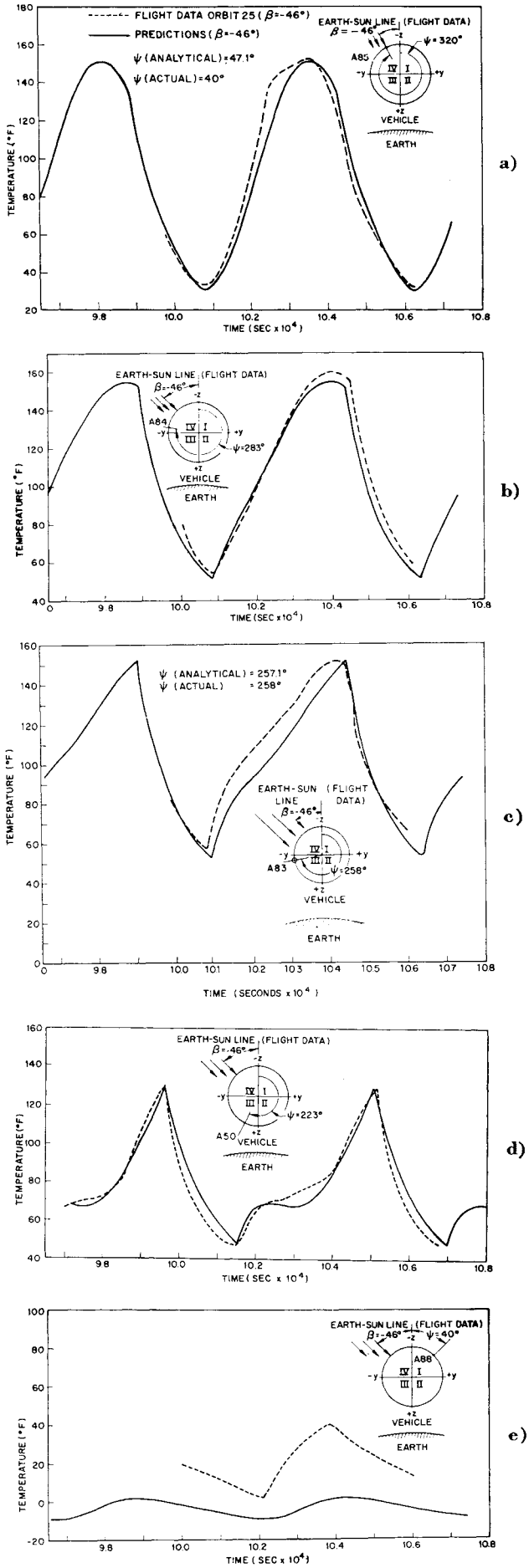

Fig. 6 Skin-temperature data comparison.

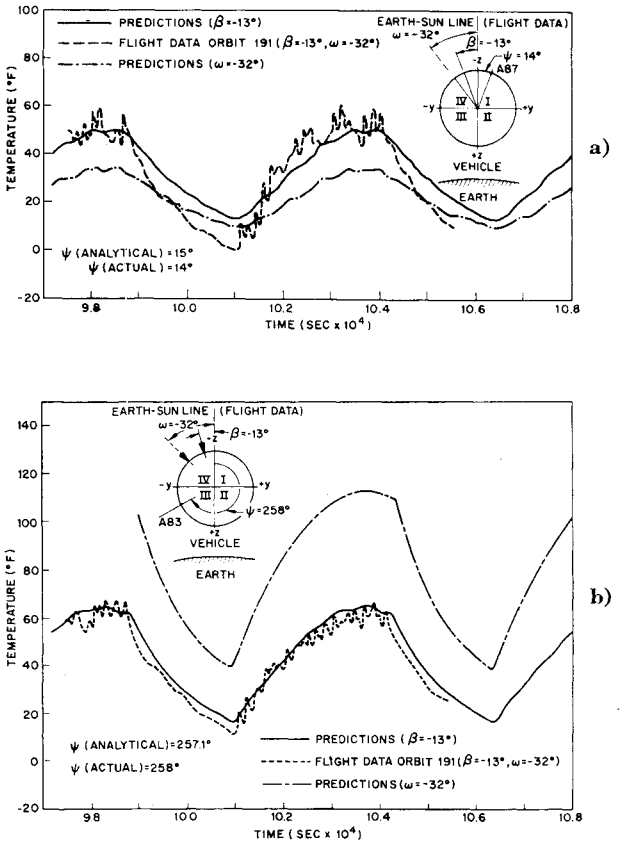

Fig. 7 Skin-temperature data comparison.

oriented. The absence of gyro telemetry during the tumbling mode precludes definitive knowledge of the vehicle dynamics; the results of the experiment as presented in this paper, however, indicate that the vehicle pitch axis did indeed remain earth-oriented. If the vehicle remained space-oriented, the angle ω, which is that angle between the solar vector and the vehicle X-X axis, would be different from β. In an earth-oriented vehicle ω and β are identical.

The data results for the tumbling mode are shown in Fig. 7 (orbit 191) for different locations on the skin. Predictions are presented for an earth-oriented pitch axis and for a space-oriented pitch axis. Figure 8 shows the two sun angles that might result. The results in Fig. 7 indicate that the pitch axis was oriented to the orbit plane. The experimental data also clearly show the effects of simultaneous pitch and the apparent oscillation in roll. Predicted temperatures based on space orientation are lower than those based on orbit orientation for the same location (Fig. 7a). This is consistent, because in the latter condition more energy would be received by the vehicle at this location. These results definitely show the effects of the pitch and roll motion as previously described. Figure 7b shows that predicted temperatures for orbit orientation correlate well with the flight-test data. At $\psi = 258°$, the surface would receive more direct solar energy and only slightly less albedo for the space-

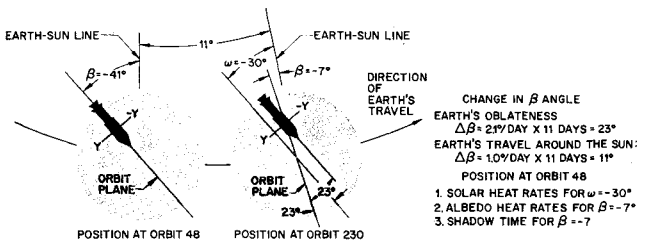

Fig. 8 Sun angle vs β, tumbling vehicle.

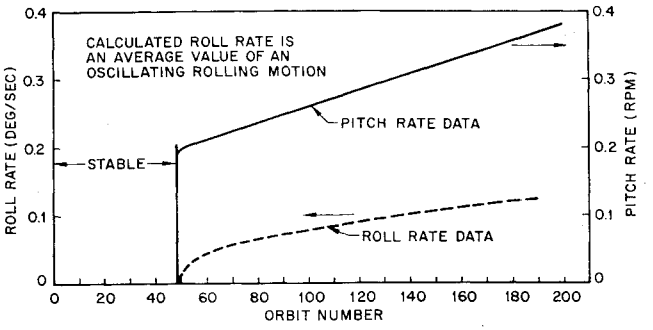

Fig. 9 Vehicle motion as determined from thermal data.

oriented (ω) case than if the vehicle were earth-oriented (β). The data from this location (Fig. 7b) provide the strongest proof of an earth-oriented flight.

Surface temperature fluctuations were used to determine the pitch and roll rates during the tumbling period of the vehicle flight. A pitch rate gyro was installed, but a calibration error resulted in failure to obtain valid data. Thermal response of the sensors was sufficient to determine the pitch rate quite precisely. Any sensor that passed between the sun vector and the pitch plane experienced a definite and regular oscillation in temperature. The "counting" of cycles resulted in the pitch rate determination shown in Fig. 9.

Roll rate determination required the method described in Fig. 10. In the data, definite discontinuities can be noted in temperature oscillation of sensors located near the sun-line tangency points. Note that sensors on opposite sides of the vehicle show different temperature slopes as expected. Point 4 on the vehicle shows a temperature sensor location in its "normal" position, without any vehicle roll. Points 1 and 3 are those in which the vehicle rolls through the tangent of the earth-sun line. Point 2 shows the extreme roll condition. The start of the discontinuity in temperature oscillation, point 1, was assumed to be where the sensor approached (entered) the tangency point (because of roll). Point 3 shows the return (note the change in slope). An extensive study of these "blips" confirmed the theory, and the roll rate was determined

$$\text{roll rate} \qquad \dot{\psi} = [2(\theta_4 - \theta_{1,3})]/(t_1 - t_3)$$

The pitch and oscillatory roll rate increased continuously, as shown in Fig. 9, possibly because of a gas leak or propellant residuals venting.

Considerable improvement could be made in obtaining the highly transient data. In this experiment, the sensors were attached to surfaces approximately 0.1 in. thick. By proper selection of sensors and mounting bases, the sensitivity of the thermal instrumentation could be improved by an order of magnitude.

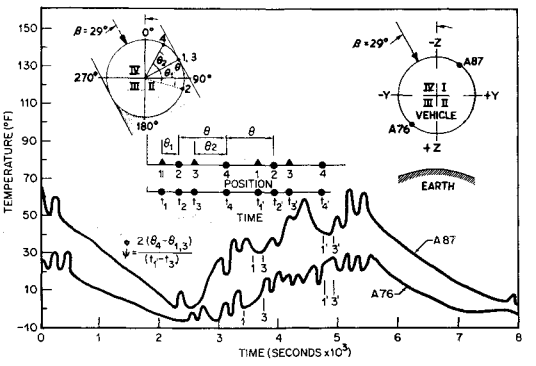

Fig. 10 Determination of roll oscillation.

Instrumentation

The thermal instrumentation selected for the experiment was based upon certain criteria, such as location, sensor type, mounting, and adaptability to the available telemetry system. The telemetry-data reduction system utilized is shown in Fig. 11 in block-diagram form. For reliability and cross-checking purposes, information from the same commutated point was received via both real-time and tape recorder. The real-time information was read out as the vehicle passed over the tracking station. Meanwhile, the same information was stored on a vehicle tape recorder to be read out on some subsequent pass. The voltage-controlled oscillators (VCO) shown in Fig. 11 were the IRIG subcarrier band 12 for the real-time and the IRIG band F for the tape recorder.

Temperature Sensors

The temperature sensors used for this flight experiment were "Micro Systems Incorporated" Model TE-3-10-1000 semiconductors. Figure 12 shows a typical resistance-vs-temperature curve. This solid-state temperature gage is a stable, linear, rapid-response, high-sensitivity, and wide-range device that is unique in the ability to provide high output and rapid response over a broad temperature range. The sensor signal conditioning, a voltage divider network, comprised a dropping resistor and a semiconductor to provide 0 to 5 av to the telemetering system from a +28-v d.c. source.

The application of the sensor to the FM/FM telemetry system consists of determining the highest value of R_t (semiconductor) anticipated for the corresponding highest temperature expected. The dropping resistor value R_d is then calculated so that, when R_t is at its maximum value (and maximum temperature), the voltage output to the telemetry system will be equal to 5 v d.c. Thus, as the temperature decreases, and correspondingly R_t decreases, the voltage output to the telemetry will decrease proportionally. The end results will be a nearly linear temperature-voltage curve.

Since the point at which zero voltage is reached does not always correspond to the lower temperature limit expected, the full 0- to 5-v bandwidth available to the telemetry system is not always utilized. The 0- to 5-v input signal can be reproduced at the output with an error accuracy of ±4% (±0.20 v) with the data reduction techniques in use. The average voltage bandwidth utilized on the temperature calibration curves for the subject vehicle was 4.0 v. Therefore, if the calibration curve is linear, the expected uncertainty of each temperature measurement can be computed accordingly to the following formula:

$$\text{uncertainty } (^\circ\text{F}) = (\Delta \text{ temperature}/\Delta \text{ voltage})(\pm 0.20 \text{ v})$$

Uncertainty was ±22°F for the subject experiment. In-flight measurements are almost impossible to check. From all of the indications, however, most of the thermal data appears to be considerably more accurate than the systems analysis would guarantee. In-flight calibration points were checked against IRIG standards to support this observation.

Table 1 Research experiment, vehicle electrical power summary

	Readin, w		Readout, w	
	Unreg.	Reg.	Unreg.	Reg.
Temperature sensor	...	1.5	...	1.5
Tape recorder	4.0	...	11.3	...
d.c-d.c. converter	8.0	...	8.0	...
Signal condition and comm.	1.8	...	1.8	...
Time-reference generator	0.5	...	0.5	...
Transmitter	...	...	19.0	...
Oscillators (3)	...	...	...	2.52
Mod. amp.	...	...	...	0.59
d.c.-d.c. converter	8.0	...	8.0	...

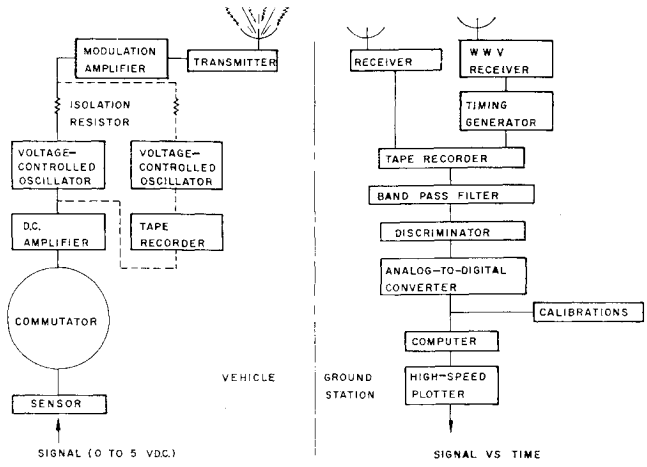

Fig. 11 Ground-space telemetry system.

Equipment Power and Weight

This experiment utilized flight-qualified equipment designed for general use in recording and transmitting data from orbiting spacecraft. Accordingly, it is recognized that power requirements and weights were not optimal. Table 1 lists the power requirements for the complete system. Approximately 600 w-hr were expended from an available 2000. The equipment total weight was 50.12 lb. As mentioned previously, this system is used on several vehicles for various types of research experiments. Accordingly, the extra weight added for this experiment, including batteries, was approximately 12 lb.

Manned Systems

The primary importance of a research experiment, such as this, is to obtain a more definitive knowledge of space effects on vehicle equipment. By doing so, the state of the art of thermal analysis can be improved, thereby adding greater reliability to the eventual manned mission. The verification of present analytical methods provides the confidence level necessary to incorporate the most important component into the spacecraft system, i.e., man. Passive thermal control surfaces coupled with an attitude control system could be used to optimize energy control for a manned vehicle. The utilization of vehicle structure and special surface finishes as the necessary heat exchanger is desired. Continuous monitoring of temperatures via telemetry-tape-recorder data systems can provide complete histories of vehicle and

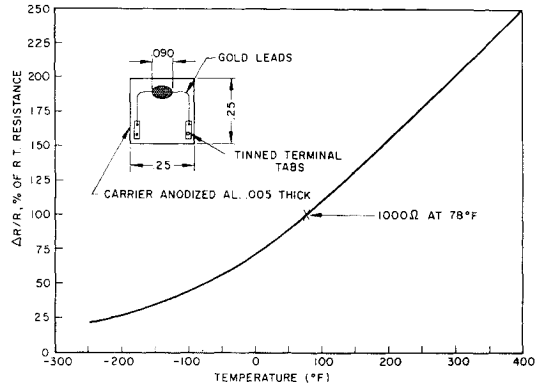

Fig. 12 Typical relative resistance vs temperature for TE-3-1000 sensor.

component equipment conditions for more realistic design and control decisions.

References

[1] Camack, W. G. and Edwards, D. K., "Surface effects on spacecraft materials," Lockheed Missiles and Space Co., LMSD 288044 (October 1959).

[2] *Space Materials Handbook*, edited by C. G. Goetzel and J. B. Singletary (Lockheed Missiles and Space Co., Sunnyvale, Calif., January 1962).

JULY-AUG. 1965 J. SPACECRAFT VOL. 2, NO. 4

Finite-Difference Solution of Two Variable Thermal and Mechanical Deformation Problems

KERRY S. HAVNER*
Douglas Aircraft Company, Inc., Santa Monica, Calif.

A numerical solution of thermoelastic stress and deformation problems governed by two linear, second-order, elliptic partial differential equations in two unknowns is presented. The analysis is applicable to both axially symmetric solids and variable thickness plates with temperature-dependent material properties. Body forces caused by rotation and/or temperature gradients and boundary conditions corresponding to any combination of prescribed tractions and displacements are considered. A general digital computer program based upon a finite-difference discretization and utilizing the method of successive overrelaxation is briefly described. Selected results from turbomachinery problems and a numerical comparison with the classical rotating ellipsoid are included.

Nomenclature

h	=	network spacing
i, j	=	network point
l, m	=	direction numbers of outward normal with respect to the R and Z axes
r, z	=	point coordinates, in.
t	=	plate thickness, in.
u, w	=	displacements in R and Z directions, respectively, in.
x, y	=	coordinates relative to boundary point in R and Z directions, respectively, in.
A_{pq}	=	general matrix element
C_1, C_2, C_3	=	dimensionless material constants
E	=	modulus of elasticity, psi
F_1, F_2	=	prescribed boundary values
F_r, F_z	=	body forces per unit volume in R and Z directions, respectively, lb/in.[3]
G	=	shear modulus, psi
T	=	temperature rise, °F
α	=	coefficient of thermal expansion, in./in./°F
α_{kl}, β_{lk}	=	matrix elements
δ_p, δ_p°	=	elements of displacement and load vectors, respectively, in.
λ	=	Lamé constant, psi $= \nu E/(1+\nu)(1-2\nu)$
ν	=	Poisson's ratio
ρ	=	mass density, lb-sec^2/in.[4]
σ_r, σ_z	=	normal stresses in R and Z directions, respectively, psi
σ_t	=	circumferential stress in axisymmetric solid, psi
τ	=	shearing stress in R-Z plane, psi
ω	=	rotational speed, rad/sec, overrelaxation factor

Received April 28, 1964; revision received October 19, 1964. The investigation upon which this paper is based was performed while the author was a member of the engineering staff of the Garrett Corporation, AiResearch Manufacturing Division, Phoenix, Ariz. R. R. VanNimwegen and Bernard Fried of the Preliminary Design Department contributed many valuable suggestions, and their encouragement and advice is gratefully acknowledged.

* Section Chief, Solid Mechanics Research, Advance Structures and Mechanical Department, Research and Development, Missile and Space Systems Division.

1. Introduction

A NUMBER of stress and deformation problems that occur in engineering practice can be represented mathematically by linear, second-order, elliptic partial differential equations. In particular, the extensional problem of the thin, variable thickness plate and the problem of the axisymmetric, three-dimensional solid can be so represented. Thus, the mathematical models of these distinctly different physical bodies, formulated in different geometries, can be incorporated within a general set of elliptic equations that includes these models as special cases.

There is a great deal to be gained by this single formulation, for the mathematical difficulties inherent in a consideration of irregular configurations, mixed boundary conditions, and the effect of thermal loading on material properties arise in both the plate and the axisymmetric solid. In such stress and deformation problems as occur in turbomachinery elements (e.g., turbine disks and blades, axisymmetric nozzles, etc.), thick-shell pressure vessels, and encased solid propellants, for example, these effects of configuration, temperature, and constraint can be quite important. Thus, some sort of discretization is mandatory if the elliptic equations to be solved are to be representative of physically significant problems. To this purpose the finite-difference method is chosen herein as the most feasible means of solution, affording considerable flexibility and enabling the development of a computer program applicable to a wide range of problems.

In recent years, numerical analyses of stress problems in irregular, thick-walled pressure vessels and encased solid propellants have been given by Thoms,[1] Conte, Miller, and Sensenig,[2] Bijlaard and Dohrmann,[3,4] and Hubka.[5] In the field of mechanical and thermal problems in rotating machinery (including blade problems) analyses have been given by Hodge and Papa,[6] Chang,[7] Schilhansl,[8] Kobayashi and Trumpler,[9] and Fried, Reichenbach, and Chingari.[10-12] The most general elasticity formulations are those by Thoms[1] and Kobayashi and Trumpler,[9] using Southwell stress functions, and Conte, Miller, and Sensenig,[2] Hubka,[5] and Fried,[12] using deformations as unknowns. The other papers make